

Isocurvature bounds on axion-like particle dark matter in the post-inflationary scenario

M. Feix,^{a,b,c} J. Frank,^d A. Pargner,^{c,d} R. Reischke,^e B.M. Schäfer,^{b,c}
T. Schwetz^{c,d}

^aInstitut für Theoretische Astrophysik, Zentrum für Astronomie der Universität Heidelberg, Philosophenweg 12, 69120 Heidelberg, Germany

^bAstronomisches Rechen-Institut, Zentrum für Astronomie der Universität Heidelberg, Philosophenweg 12, 69120 Heidelberg, Germany

^cHEiKA – Heidelberg Karlsruhe Research Partnership, Heidelberg University, Karlsruhe Institute of Technology (KIT), Germany

^dInstitut für Kernphysik, Karlsruher Institut für Technologie (KIT), Hermann-von-Helmholtz-Platz 1, 76344 Eggenstein-Leopoldshafen, Germany

^eDepartment of Physics, Israel Institute of Technology – Technion, 3200003 Haifa, Israel

E-mail: feix@uni-heidelberg.de, r.reischke@campus.technion.ac.il, andreas.pargner@kit.edu

Abstract. We assume that dark matter is comprised of axion-like particles (ALPs) generated by the realignment mechanism in the post-inflationary scenario. This leads to isocurvature fluctuations with an amplitude of order one for scales comparable to the horizon at the time when the ALP field starts oscillating. The power spectrum of these fluctuations is flat for small wave numbers, extending to scales relevant for cosmological observables. Denoting the relative isocurvature amplitude at $k_* = 0.05 \text{ Mpc}^{-1}$ by f_{iso} , Planck observations of the cosmic microwave background (CMB) yield $f_{\text{iso}} < 0.31$ at the 2σ -level. This excludes the hypothesis of post-inflationary ALP dark matter with masses $m_a < 10^{-20} - 10^{-16} \text{ eV}$, where the range is due to details of the ALP mass-temperature dependence. Future CMB stage IV and 21-cm intensity mapping experiments may improve these limits by 1–2 orders of magnitude in m_a .

Keywords: axions, cosmological parameters from LSS, dark matter theory

Contents

1	Introduction	1
2	ALPs in the post-inflationary symmetry breaking scenario	3
2.1	Cosmic evolution	4
2.2	Relic density	5
2.3	Initial isocurvature power spectrum	6
2.4	Assumptions and uncertainties	7
3	Constraints from cosmic large-scale structure	9
3.1	Large-scale imprint of isocurvature fluctuations	9
3.2	CMB experiments	11
3.3	HI intensity mapping	12
4	Results	14
4.1	Bounds on the isocurvature amplitude	14
4.2	Implications for ALP masses	17
5	Discussion and conclusion	19

1 Introduction

Over the last decades, the increasing wealth of astronomical data has firmly established the standard cosmological paradigm where the observed cosmic structure has formed out of small perturbations in the primordial energy-matter density field and their subsequent growth due to gravitational interaction. Interpreted within general relativity (GR), the gathered evidence for a mass deficit of visible matter on astrophysical and cosmological scales [1, 2] as well as strong indications for an accelerated expansion of the Universe [3–5] have led to the now widely accepted cold dark matter (DM) model with a cosmological constant, usually denoted as the Λ CDM model [e.g., 6]. Originally invoked to explain the observed dynamics of galaxies within the Coma cluster [7, 8], DM remains merely a postulate of the cosmological model and its true nature is unarguably one of the largest puzzles in modern physics.

A well-motivated particle physics candidate for DM is the axion [9–12] which appears as a pseudo-Nambu-Goldstone boson (PNGB) in the Peccei-Quinn (PQ) solution to the strong CP problem [13]. Their solution introduces a new global chiral $U(1)$ symmetry that gets spontaneously broken at some energy scale f_a by the vacuum expectation value of a complex scalar field. The axion then emerges as the phase degree of freedom of this complex scalar. To satisfy current experimental bounds, f_a can be assumed very large. This gives the axion very weak interactions and an extremely small mass [14–17]. There exist many other high-energy extensions of the standard model that also contain PNGBs sharing properties similar to those of the axion. These are commonly referred to as axion-like particles (ALPs) [18–20].

Despite their low masses, axions and ALPs can effectively mimic the properties of a (cold) DM component, thanks to the possibility of non-thermal production via the vacuum realignment mechanism [21–24]. At early times when the temperature $T \sim f_a$, the axion (or ALP) field is essentially massless. Since no specific field value is energetically favoured

in this case, it simply takes a random one. At lower temperatures around the QCD phase transition, however, its potential becomes important, causing the axion field to roll down to the CP conserving minimum and, therefore, realign with the vacuum. The energy stored in the coherent oscillations around this minimum then largely behaves like collisionless DM on cosmologically relevant scales. Considering the QCD axion, a typical mass suitable to explain the observed DM density is $m_a \sim 10^{-5}$ eV [25–27]. For ALPs, there is substantially more freedom in the allowed mass range which may extend to much smaller values [e.g. 19].

There exist two fundamentally different scenarios depending on how the vacuum realignment mechanism is realized in the early Universe. If the PQ symmetry is broken before (or during) an inflationary epoch, the axion (or ALP) field takes a single value in the whole observable Universe that sets its energy density in an evenly distributed manner. However, if PQ symmetry breaking happens after the end of inflation, the situation becomes more involved. In this case, the axion field generally takes different values in causally disconnected regions, giving rise to large isocurvature fluctuations in the axion energy density field. This has interesting phenomenological consequences for axion DM, in particular the formation of gravitationally bound objects known as miniclusters [28–35].

In contrast to the QCD axion, the presence of ultra-light ALPs (ULAs) can have a sizable and potentially measurable effect on cosmological large-scale observables. For instance, observations of the cosmic microwave background (CMB) anisotropy spectrum and large galaxy surveys have already been used to constrain ULAs, essentially excluding ULA masses within the range 10^{-32} eV $< m_a < 10^{-25}$ eV [36–40].¹ Considering smaller (non-linear) scales, comparisons of the observed Lyman- α flux power spectrum with predictions based on hydrodynamical simulations suggest an increased lower bound of $m_a \gtrsim 10^{-21}$ eV [41, 42]. Even tighter constraints may be obtained by introducing additional assumptions, for instance, from the formation of solitonic cores in DM halos [43] or from the spin-down of super-massive black holes via superradiant instability [e.g., 44, 45].

While it is well-known that observational bounds on isocurvature fluctuations in the axion field generated during inflation [46] constrain the *pre-inflationary PQ breaking scenario* [e.g., 47–53], we will show in the present work that similar isocurvature constraints also apply in the *post-inflationary PQ breaking scenario*. To this end, we will consider the more general context of ALPs and assume that the vacuum realignment mechanism is the most relevant production mechanism of such particles in the early Universe. In addition to adiabatic modes, this scenario generically predicts cosmological isocurvature fluctuations that are characterized by a much steeper power spectrum than the usually assumed (nearly) scale-invariant spectrum produced during inflation. The origin of these isocurvature fluctuations is the large inhomogeneity of the ALP field between causally disconnected regions at the time when the field starts to oscillate and behaves as DM. By looking at their corresponding imprints on CMB temperature anisotropies and the matter power spectrum, we will be able to place constraints on large parts of the parameter space where such ALPs constitute the cosmic DM, thereby complementing existing and predicted bounds on ULA masses from current and future large-scale experiments, respectively. In particular, we will focus on constraints based on Planck data [5, 54], and provide forecasts for next-generation CMB [e.g., 55, 56] and HI intensity mapping experiments such as the Square Kilometre Array (SKA) [57–59].

This work is structured as follows: in [section 2](#), we introduce our model for ALP DM

¹Note that ULAs with masses $m_a \lesssim 10^{-27}$ eV cannot account for all of the observed DM in the Universe since field oscillations would commence only after matter-radiation equality, and axions would mainly manifest as a dark energy component.

in the context of post-inflationary PQ breaking. Assuming that ALPs are mainly produced through the vacuum realignment mechanism, we present estimates of the cosmological relic abundance as well as the initial power spectrum of isocurvature fluctuations. The latter’s effect on CMB anisotropies and the matter power spectrum is discussed in [section 3](#), and then used to derive strong limits on ULA DM based on current and future large-scale datasets in [section 4](#). We conclude and summarize our findings in [section 5](#).

Throughout, we will assume a spatially flat reference cosmology based on [\[60\]](#), adopting the total matter density parameter $\Omega_{\text{m}} = 0.315$, the baryon density parameter $\Omega_{\text{b}} = 0.049$, the amplitude $A_{\text{s}} = 2.215 \times 10^{-9}$ of the primordial adiabatic spectrum, its spectral index $n_{\text{s}} = 0.9603$ (without running, i.e. $\alpha_{\text{s}} = 0$), the optical depth $\tau = 0.089$, the dimensionless Hubble parameter $h = 0.673$, and the sum of neutrino masses $\sum m_{\nu} = 0.05$ eV. Additional parameters relevant to our analysis will be introduced and specified below.

2 ALPs in the post-inflationary symmetry breaking scenario

In what follows, we consider the cosmological evolution of ALP fields in the post-inflationary PQ breaking scenario. Building on semi-analytical results obtained for the QCD axion in [\[34\]](#), we adopt the harmonic approximation for the potential and focus on the vacuum realignment mechanism which constitutes a largely model-independent way of producing relic axions in the early Universe [\[21–24, 61\]](#).

A key difference between QCD axions and ALPs is that the latter do not necessarily exhibit a specific relation between mass, m_a , and breaking scale, f_a . Assuming that a potential for the ALP field a is generated by some exotic strongly interacting sector, we may write

$$V(a) \approx \Lambda^4 \left[1 - \cos \left(\frac{a}{f_a} \right) \right], \quad m_a^2 = \left. \frac{\partial^2 V}{\partial a^2} \right|_{\text{min}} = \frac{\Lambda^4}{f_a^2}, \quad (2.1)$$

where, in analogy to the instanton potential of QCD axions, Λ^4 takes the role of a topological susceptibility χ that is generally model-dependent and will be parametrized below. Hence, the ALP is characterized by two out of the three parameters f_a , m_a , and Λ .

A crucial ingredient for the cosmological evolution of ALPs is the temperature dependence of its mass. For the QCD axion, this is fully determined by non-perturbative QCD effects [see, e.g., [62, 63](#)]. For general ALPs, however, it depends on the specifics of the mechanism generating their mass. In the following, we will assume a power law that turns into the constant zero-temperature mass $m_a = \Lambda^2/f_a$ for low temperatures,

$$m_a(T) = \min \left[\frac{\Lambda^2}{f_a}, b \frac{\Lambda^2}{f_a} \left(\frac{\Lambda}{T} \right)^n \right], \quad (2.2)$$

where the parameter b accounts for the possibility that the zero-temperature mass might not exactly be reached at $T = \Lambda$, but at

$$T_0 = b^{1/n} \Lambda. \quad (2.3)$$

We will consider values in the range $b \simeq 0.1\text{--}10$. The parameter $n \in \mathbb{R}_+$ controls how quickly the mass emerges. Choosing $\Lambda = 75.5$ MeV, $b = 10$, and $n = 4$, [eq. \(2.2\)](#) reproduces the $m_a(T)$ -behaviour for the QCD axion as obtained in [\[62\]](#) to good accuracy.

2.1 Cosmic evolution

The evolution of the (real) ALP scalar field in an expanding universe, expressed in terms of the angular field $\theta(\mathbf{x}) = a(\mathbf{x})/f_a$, is governed by the action

$$S_\theta = \int d^4x \sqrt{-g} f_a^2 \left[-\frac{1}{2} (\nabla_\mu \theta) (\nabla^\mu \theta) - V(\theta) \right], \quad (2.4)$$

where g is the determinant of the well-known Friedmann-Lemaître-Robertson-Walker space-time metric $g_{\mu\nu}$ (with signature $+2$), and

$$V(\theta, T) = m_a^2(T) (1 - \cos \theta) \quad (2.5)$$

is the temperature-dependent ALP potential. Variation of [eq. \(2.4\)](#) with respect to $\theta(\mathbf{x})$ yields the equation of motion,

$$\ddot{\theta} + 3H\dot{\theta} - \frac{1}{R^2} \nabla^2 \theta + \frac{dV}{d\theta} = 0, \quad (2.6)$$

where R is the cosmic scale factor, $H = \dot{R}/R$ denotes the Hubble parameter, dots correspond to derivatives with respect to time, and ∇ is defined with respect to comoving coordinates. At early times, well before matter-radiation equality, the contribution of ALPs to the total energy density budget of the Universe is minuscule, and we will assume that its impact on the cosmic expansion can be neglected. As usual, the field's energy density, ρ_a (and similarly, its pressure) can be computed from the stress-energy tensor and is given by

$$\rho_a = f_a^2 \left[\frac{1}{2} \dot{\theta}^2 + \frac{1}{2R^2} (\nabla \theta)^2 + V(\theta) \right]. \quad (2.7)$$

The periodic form of the potential renders the cosmic evolution nonlinear and severely complicates its analysis. To make analytic progress, however, we assume that the potential may be approximated as $V(\theta, T) \simeq m_a^2(T) \theta^2/2$. Although this ignores potentially important effects such as the formation of strings and domain walls [\[64\]](#) or the emergence of very dense objects in the context of miniclusters [\[29, 30\]](#), we will obtain useful estimates for ALP DM on the large scales relevant to cosmological probes. We further discuss this issue in [section 2.4](#).

Within the harmonic approximation, [eq. \(2.6\)](#) expressed in Fourier space reduces to

$$\ddot{\theta}_{\mathbf{k}} + 3H(T)\dot{\theta}_{\mathbf{k}} + \omega_{\mathbf{k}}^2 \theta_{\mathbf{k}} = 0, \quad \omega_{\mathbf{k}}^2 = \frac{k^2}{R^2} + m_a^2(T), \quad (2.8)$$

which is reminiscent of the damped harmonic oscillator. At high temperatures, the ALP field is essentially massless. Ignoring decaying solutions, we see from [eq. \(2.8\)](#) that $\theta_{\mathbf{k}} = \text{const}$ for superhorizon modes with $\omega_{\mathbf{k}} \ll 3H$. Upon entering the horizon, these modes will start oscillating. To characterize this transition, we introduce T_{osc} as the temperature where the zero-mode starts to oscillate,

$$3H(T_{\text{osc}}) = m_a(T_{\text{osc}}). \quad (2.9)$$

For all modes, the mass term will eventually dominate at late times, and the ALP energy density given by [eq. \(2.7\)](#) will behave like cold DM. The Hubble rate during radiation domination is given by

$$H(T) \approx 1.66 \sqrt{g_*(T)} \frac{T^2}{M_P}, \quad (2.10)$$

where g_* denotes the effective number of relativistic degrees of freedom and M_P the Planck mass. With the parametrization from eq. (2.2) for $m_a(T)$, we can estimate

$$T_{\text{osc}} \sim \Lambda \left(\frac{b}{\sqrt{g_*(T_{\text{osc}})}} \frac{M_P}{f_a} \right)^{1/(2+n)}. \quad (2.11)$$

Using that $\sqrt{g_*(T_{\text{osc}})} \simeq \text{few}$ and comparing with eq. (2.3), we see that for reasonable values of b and n , we have $T_{\text{osc}}/T_0 \sim (M_P/f_a)^{1/(2+n)}$. Hence, the condition $f_a \ll M_P$ implies that the ALP field starts oscillating before reaching its zero-temperature mass. Therefore, the details of the temperature dependence are important and our results will depend to some extent on the parameters b and n . For our calculations, we solve eq. (2.9) numerically by interpolating the effective degrees of freedom tabulated as a function of temperature from [62], extended to temperatures below MeV by using the results of [65].

2.2 Relic density

To estimate the cosmological mean density, we note that contributions from modes with $|\mathbf{k}| \neq 0$ will be quickly suppressed relative to the zero mode due to the factor R^{-2} appearing in $\omega_{\mathbf{k}}^2$. Considering only the zero mode (which is equivalent to dropping the gradient terms in the evolution equation), using a WKB ansatz allows one to obtain an approximate expression for the cosmic mean density valid for temperatures $T < T_{\text{osc}}$ [21–25],

$$\bar{\rho}_a(T) \simeq \frac{1}{2} f_a^2 m_a(T_{\text{osc}}) m_a(T) \left[\frac{R(T_{\text{osc}})}{R(T)} \right]^3 \langle \theta_{\text{ini}}^2 \rangle, \quad (2.12)$$

where $\langle \theta_{\text{ini}}^2 \rangle = \pi^2/3$ is the mean value of θ_{ini}^2 averaged over many different Hubble patches around $T = T_{\text{osc}}$. A more rigorous approach is to directly solve the system given by eq. (2.8) for all relevant modes. Rewriting $\theta_{\mathbf{k}}(R) = \theta_{\mathbf{k}}^i f_{\mathbf{k}}(R)$, where $\theta_{\mathbf{k}}^i$ is the initial value at time t_i and $f_{\mathbf{k}}(R)$ captures its evolution with $f_{\mathbf{k}}(R_i) = 1$, the mean energy density can be formally related to the field’s initial power spectrum $P_\theta(k)$,

$$\bar{\rho}_a = \frac{f_a^2}{2} \int_0^\infty \frac{d^3k}{(2\pi)^3} P_\theta(k) F(\mathbf{k}, \mathbf{k}), \quad (2.13)$$

where $\theta(\mathbf{x})$ is assumed as statistically homogeneous and isotropic, $P_\theta(k)$ is defined through $\langle \theta_{\mathbf{k}} \theta_{\mathbf{k}'}^* \rangle = (2\pi)^3 \delta_D(\mathbf{k} - \mathbf{k}') P_\theta(k)$, and

$$F(\mathbf{k}, \mathbf{k}') = \dot{f}_{\mathbf{k}} \dot{f}_{\mathbf{k}'} + \left[\frac{\mathbf{k} \cdot \mathbf{k}'}{R^2} + m_a(T) \right] f_{\mathbf{k}} f_{\mathbf{k}'}. \quad (2.14)$$

The expression in eq. (2.13) is of the same parametric form as eq. (2.12), but replaces $\langle \theta_{\text{ini}}^2 \rangle = \pi^2/3$ with a proper weighted contribution of non-zero modes specified by $P_\theta(k)$ [34].

In the post-inflationary scenario, the ALP field θ will assume uncorrelated values in causally disconnected regions whereas the gradient terms in the evolution equation tend to equalize the value of θ inside the horizon [64] (see, e.g., [66] for recent simulations). This can be described by an initial power spectrum $P_\theta(k)$ corresponding to a constant (i.e. white noise) for $k < RH$, whereas power for $k > RH$ is suppressed. Here “initial” means shortly before the ALP field starts to oscillate. Following [34], we choose an exponential shape for the power spectrum, $P_\theta(k) \propto \exp(-k/Q)$ with $Q = R_i H(T = T_i)$, and set the initial time

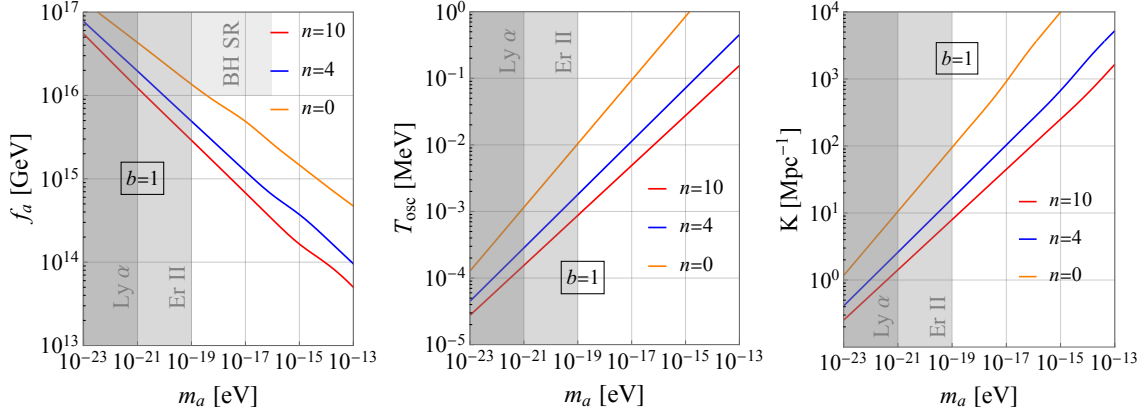


Figure 1. The left panel shows f_a -values that yield the correct DM abundance according to eq. (2.13) as a function of m_a . These f_a -values are assumed for the other two panels. The middle panel illustrates T_{osc} as a function of m_a , and the right panel shows the comoving wave number corresponding to the horizon at $T = T_{\text{osc}}$. Shaded areas indicate constraints on the axion mass from the Lyman- α forest [41, 42], solitonic core formation in Eridanus II [43], and the spin-down of super-massive black holes via superradiant instability [45]. The latter constraint is only shown in the left panel as these bounds disappear for $f_a \lesssim 10^{16}$ GeV due to ALP self-interactions [44].

to $T_i = 3T_{\text{osc}}$. The amplitude of the power spectrum for $k \ll Q$ is fixed by requiring that $\langle \theta^2 \rangle = \pi^2/3$.

To determine $f_{\mathbf{k}}(t)$, we approach the equation of motion numerically. We use a realistic temperature dependence of g_* from [62, 65], and solve eq. (2.9) for temperatures from T_i down to a few times less than T_{osc} . This solution is then matched onto a WKB approximation for lower temperatures to factor out the fast oscillations of the axion field (see [34] for details). For a given temperature dependence of the ALP mass, we can calculate the energy density using eq. (2.13).

Requiring that ALPs provide all of the DM fixes f_a for given values of m_a . This is shown in the left panel of figure 1 for various choices of n and $b = 1$. Using the approximate formula for the energy density, eq. (2.12), we can qualitatively estimate the behaviour as

$$f_a \propto b^{2/(8+3n)} m_a^{-(2+n)/(8+3n)}, \quad (2.15)$$

where we ignore a mild dependence of the proportionality constant on n . Considering the large- and small- n limit we find $f_a \propto m_a^{-1/4}$ for $n = 0$, and $f_a \propto m_a^{-1/3}$ for $n \gg 1$. In the middle panel of the figure, we show T_{osc} as a function of m_a , adopting values of f_a that yield the correct DM abundance as shown in the left panel. Qualitatively, we find $T_{\text{osc}} \propto m_a^{1/2}$ for $n = 0$, and $T_{\text{osc}} \propto m_a^{1/3}$ for $n \gg 1$. For the relevant region of parameter space, we see that T_{osc} is always much larger than the temperature at matter-radiation equality, $T_{\text{eq}} \sim \text{few eV}$. Hence, the ALP fields becomes matter-like early enough to explain the DM in the Universe.

2.3 Initial isocurvature power spectrum

The random initial ALP field values in different Hubble patches will lead to large variations in the energy density. Qualitatively, we expect order-one density fluctuations between regions

of the size of the horizon at the time when ALP DM is born, i.e. at $T = T_{\text{osc}}$ [28]. Densities in causally disconnected regions at that time will be statistically uncorrelated. Let us denote the comoving wave number corresponding to the horizon at $T = T_{\text{osc}}$ by

$$K = R_{\text{osc}}H(T_{\text{osc}}). \quad (2.16)$$

We then expect a constant power spectrum (white noise) of the ALP energy density for $k < K$, with a cutoff around $k \simeq K$. Hence, the dimensionless power spectrum, Δ^2 , can be parametrized as

$$\Delta^2(k) \equiv \frac{k^3}{2\pi^2}P(k) = C \left(\frac{k}{K} \right)^3 \quad (k \lesssim K). \quad (2.17)$$

For C of $\mathcal{O}(1)$, the variance of the density fluctuations at scales comparable to the horizon at T_{osc} is also of $\mathcal{O}(1)$. The shape of the power spectrum for $k \sim K$ will be complicated and depends on the details of the dynamics at temperatures around T_{osc} . In the following, however, we will be interested in length scales much larger than the horizon at T_{osc} , i.e. $k \ll K$. Thus, we do not need to know the precise shape around the cutoff, and the parametrization eq. (2.17) will be an excellent approximation for the scales of interest. Typical values of K are shown in the right panel of figure 1. During radiation domination, we approximately have $R \propto T^{-1}$ and $H \propto T^2$, and using eq. (2.16) yields $K \propto T_{\text{osc}}$. Therefore, K and T_{osc} have the same dependence on m_a , as is transparent from figure 1.

To estimate C , the normalization constant of the power spectrum, we proceed as follows. Using the result of [34], the energy density power spectrum is obtained in terms of the ALP field's initial power spectrum as

$$P(k) = 2(2\pi)^3 \frac{\int d^3k' P_\theta(|\mathbf{k}'|)P_\theta(|\mathbf{k} - \mathbf{k}'|)F(\mathbf{k}', \mathbf{k}' - \mathbf{k})^2}{\left[\int d^3k' P_\theta(k')F(\mathbf{k}', \mathbf{k}') \right]^2}, \quad (2.18)$$

with $F(\mathbf{k}, \mathbf{k}')$ given by eq. (2.14). Solving the ALP field's equations of motion to determine $f_{\mathbf{k}}(t)$, we find that the power spectrum calculated according to eq. (2.18) becomes constant in time shortly after T_{osc} , as soon as the mass term dominates over the k -term in eq. (2.14). Writing eq. (2.17) as $P(k) = 2\pi^2 C/K^3$, we obtain C from the limit $k \rightarrow 0$ in eq. (2.18). Depending on the parameters m_a , f_a , n , and b , we arrive at values $0.04 \lesssim C \lesssim 0.3$.

The important observation is that these density fluctuations are of isocurvature type since they arise only in the DM fluid. We will use that these fluctuations are also present at length scales relevant to CMB observations. As is seen from the right panel of figure 1, the spectrum's cutoff scale is much larger than scales probed by the CMB, $k_{\text{CMB}} \ll K$. Since we are far away from the cutoff, the parametrization eq. (2.17) will give an accurate description of the isocurvature power spectrum. For given values of m_a , n , and b (f_a fixed by assuming that ALPs constitute all DM), we can predict the amplitude of the white noise power spectrum as outlined above, and test whether CMB observations are compatible with the presence of such an isocurvature component.

2.4 Assumptions and uncertainties

Harmonic approximation of the ALP potential. The assumptions and limitations of our approach are discussed in [34]. Let us briefly comment on the main uncertainties of our calculations and compare them to other studies in the literature. An important assumption is the harmonic approximation of the ALP potential which removes the periodic nature of

the ALP field. Therefore, we neglect the formation of cosmic strings and domain walls as well as contributions to the ALP energy density from the decay of these topological defects shortly after the field starts oscillating.² These phenomena have been studied in some detail in the context of the QCD axion [see, e.g., 26, 27, 35, 66–68]. Although the contribution of topological defects to the energy density can be substantial, there is no general consensus on its quantitative size. This introduces an uncertainty of $\mathcal{O}(1)$ in our estimate of the ALP energy density.

Further, the nonlinear structure of the field may also play an important role in the power spectrum of density fluctuations. This has been recently studied in detail by numerical simulations including the full periodic axion potential [35]. Qualitatively, the picture obtained in this work agrees with the results of [34] for $k \ll K$. In particular, it confirms the white noise power spectrum and supports our parametrization eq. (2.17), including the extrapolation to small k -values. Quantitatively, there are some differences regarding the value of the coefficient C appearing in eq. (2.17). Choosing values for m_a , n , and b that correspond to the QCD axion, our method yields $C \approx 0.15 - 0.16$ whereas the analysis of [35] obtains $C = 0.03 \pm 0.01$, approximately a factor 5 smaller than our semi-analytical result. We will use this as an estimate for the systematic uncertainty in our prediction for the amplitude of the isocurvature power spectrum. Below we will show results for C -values ranging from our estimate based on eq. (2.18) to values that are 5 times smaller.

Note that the model dependence of $m_a(T)$ parametrized by b and n introduces an uncertainty of similar size or larger. Also, our choices of the cutoff Q in the initial power spectrum $P_\theta(k)$ as well as of the initial time ($T_i = 3T_{\text{osc}}$) are somewhat arbitrary and introduce further numerical uncertainties on the value of C (see [34] for a detailed discussion and some quantitative estimates). To summarize, although our method to compute the ALP energy density and the power spectrum is clearly approximate, it leads to an order-of-magnitude estimate consistent with numerical simulations. Given the even larger uncertainty due to the ALP model dependence, we thus proceed with our estimates.

Post-inflationary assumption. In our work, we always assume that the ALP field takes random values in causally disconnected regions at temperatures well above T_{osc} . This implies that the PQ symmetry is broken after the end of inflation or restored at some point thereafter. The condition for this so-called *post-inflationary scenario* is [50]

$$f_a < \max[T_{\text{GH}}, T_{\text{max}}]. \quad (2.19)$$

Here the Gibbons-Hawking temperature is defined by $T_{\text{GH}} = H_I/2\pi$, where H_I is the Hubble parameter during inflation, and $T_{\text{max}} = \epsilon_{\text{eff}} E_I$ is the maximal temperature after inflation, with E_I denoting the energy scale of inflation, and ϵ_{eff} is a dimensionless efficiency parameter with $0 < \epsilon_{\text{eff}} < 1$. Using $H_I = \sqrt{8\pi/3} E_I^2/M_P$, we have $T_{\text{max}} = \epsilon_{\text{eff}} (3\pi/2)^{1/4} \sqrt{T_{\text{GH}} M_P}$, which can be larger than T_{GH} for $\epsilon_{\text{eff}} \simeq 1$.

Under the assumption of slow-roll inflation driven by a single scalar field with canonical kinetic term, CMB data sets an upper limit on E_I through the non-detection of primordial tensor modes, $E_I < 1.7 \times 10^{16}$ GeV (95% CL) [46], which implies $T_{\text{GH}} < 1.1 \times 10^{13}$ GeV. Adopting this constraint, the left panel of figure 1 indicates that the condition $f_a < T_{\text{max}}$ can be met in the relevant parameter region for $m_a \gtrsim 10^{-19}$ eV, assuming $\epsilon_{\text{eff}} \gtrsim 0.1$. A less model-dependent bound on the scale of inflation has been derived in [69] using large-scale

²Note, however, that the existence of topological defects during the early field evolution is a crucial ingredient for producing large fluctuations in the axion field [64].

isotropy: $H_I < 10^{-4} M_P$. This leads to upper bounds on T_{GH} and T_{max} about one order of magnitude larger than the ones quoted above.

In summary, the condition [eq. \(2.19\)](#) for the post-inflationary scenario can be satisfied under reasonable assumptions on inflation in the region of ALP parameters that are of interest to us. As this generally requires high values of E_I , we expect relatively large tensor-to-scalar ratios in such scenarios, likely to be in the observable range in the near future (with some inflationary model-dependence).

3 Constraints from cosmic large-scale structure

3.1 Large-scale imprint of isocurvature fluctuations

Fluctuations in the ALP density will affect the initial conditions of structure formation and their subsequent evolution through gravitational instability. In what follows, we assume linear theory and focus on scalar perturbations to describe their imprint on CMB anisotropies and the matter power spectrum. The initial perturbations are set deep within the radiation era where all modes of interest are well outside the horizon. Adopting the comoving (total-matter) gauge, the standard initial conditions for adiabatic modes are related to the primordial spatial curvature perturbation, \mathcal{R} , generated by inflation through [e.g., [70](#)]

$$\delta_{\mathbf{k}} = \frac{4}{9} \frac{1 + (2/5)X_\nu}{1 + (4/15)X_\nu} \left(\frac{k}{RH} \right)^2 \mathcal{R}_{\mathbf{k}}, \quad X_\nu = \frac{\rho_\nu}{\rho_\gamma + \rho_\nu}, \quad (3.1)$$

where $\delta = \delta\rho/\rho$ is the total density contrast, ρ_γ and ρ_ν are the energy densities of photons and neutrinos, respectively, and $X_\nu = (7/8)(4/11)^{4/3} N_{\text{eff}} \approx 0.69$ for an effective number of neutrino species $N_{\text{eff}} = 3.046$. Adiabatic perturbations in single fluid components i characterized by equation-of-state parameters w_i satisfy

$$\frac{\delta_i^{\text{ad}}}{1 + w_i} = \frac{3}{4} \delta^{\text{ad}} \quad (\text{adiabatic mode}). \quad (3.2)$$

As usual, we assume that $\Delta_{\mathcal{R}}^2$ takes the form of a nearly scale-invariant spectrum parametrized by

$$\Delta_{\mathcal{R}}^2 = A_s \left(\frac{k}{k_*} \right)^{n_s - 1}, \quad n_s \approx 1, \quad (3.3)$$

where the amplitude A_s is defined with respect to the pivot scale $k_* = 0.05 \text{ Mpc}^{-1}$.

In addition to the adiabatic mode, the breaking of the PQ symmetry after inflation will induce isocurvature perturbations in the ALP field (see [section 2.3](#)). These may be written in terms of an initial entropy perturbation, \mathcal{S}_a , defined relative to the photon component,

$$\mathcal{S}_a = \frac{\delta_a}{1 + w_a} - \frac{3}{4} \delta_\gamma = \frac{\delta_a^{\text{iso}}}{1 + w_a} - \frac{3}{4} \delta_\gamma^{\text{iso}} \approx \delta_a^{\text{iso}} - \frac{3}{4} \delta_\gamma^{\text{iso}} \approx \delta_a^{\text{iso}}, \quad (3.4)$$

where we again assumed radiation domination, and the last step follows from the general isocurvature condition $\sum_i \delta\rho_i^{\text{iso}} = 0$ [e.g., [70](#)]. In [eq. \(3.4\)](#), we have also set $w_a \approx 0$, i.e. for the purposes of this work, we will use that the evolution of perturbations in the ALP field can be approximated by that of a cold DM component. Although changes in w_a are important at very early times, the ALP field quickly adopts the behaviour of pressureless matter as soon as $T \lesssim T_{\text{osc}}$. If the oscillations commence sufficiently deep within the radiation era, ALPs

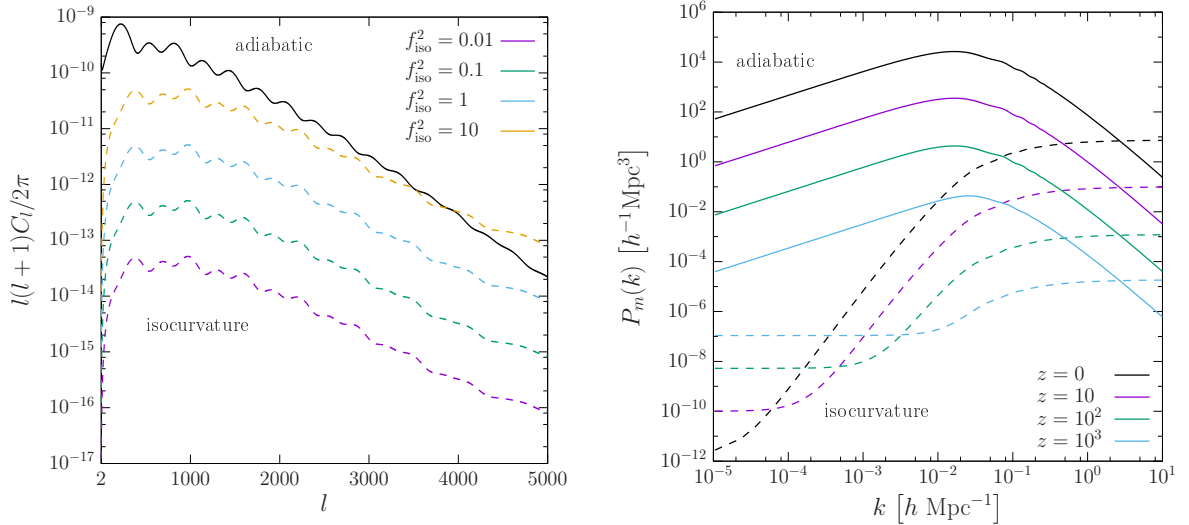


Figure 2. Imprint of ALP DM isocurvature fluctuations (generated after inflation; dotted lines) on CMB anisotropies (unlensed; left) and the linear matter power spectrum, $P_m(k)$, at various redshifts $0 \leq z \leq 10^3$ for $f_{\text{iso}} = 0.1$ (expressed in comoving gauge; right). Results for the adiabatic mode are shown as solid lines. As isocurvature and adiabatic modes are uncorrelated, total spectra are obtained by adding their individual contributions.

can effectively be treated as a cosmic matter fluid, with initial conditions set by eqs. (3.1) and (3.4). Even so, the ALP field will exhibit an effective sound speed [71, 72],

$$c_s^2 = \frac{k^2}{k^2 + 4m_a^2 R^2}, \quad (3.5)$$

that introduces a corresponding Jeans scale, k_J , below which the evolution of ALP density perturbations significantly differs from standard cold DM. Therefore, we must additionally require $k \ll k_J$. Considering scales relevant to CMB observations, it turns out that both of the above criteria are already well satisfied for ALPs with $m_a \gtrsim 10^{-24}$ eV [39, 40, 72]. Since the lower bounds on m_a implied by the energy scale of inflation lie above this threshold (see section 2.4), our approximate treatment is justified.

As discussed in section 2.3, the initial isocurvature spectrum, Δ_S^2 , is then specified by eq. (2.17), where the cutoff at $k \sim K$ can be safely ignored for practical purposes and is formally shifted to infinity.³ Hence the ALP DM isocurvature mode is completely characterized by the amplitude of Δ_S^2 which is commonly parametrized in terms of the entropy-to-curvature ratio, f_{iso} , defined at the pivot scale,

$$f_{\text{iso}}^2 \equiv \frac{\Delta_S^2}{\Delta_{\mathcal{R}}^2} \Big|_{k=k_*}. \quad (3.6)$$

In this work, we will derive constraints on f_{iso} based on Planck observations [5, 54] and adopt the Fisher matrix formalism [73] to obtain forecasts for future CMB and 21-cm experiments.

³For the smallest masses considered here, this and the treatment of ALPs in terms of a cold DM component strictly hold on CMB scales only. As we shall see shortly, however, current CMB data imply $m_a \gtrsim 10^{-20}$ eV, which allows us to use these assumptions on smaller scales $k \lesssim 1\text{--}10 h \text{ Mpc}^{-1}$ as well.

ν [GHz]	θ_{beam} [arcmin]	σ_T [$\mu\text{K arcmin}$]	σ_P [$\mu\text{K arcmin}$]
90	5.7	18.80	26.6
105	4.8	13.80	19.6
135	3.8	9.85	13.9
160	3.2	7.78	11.0
185	2.8	7.05	9.97
200	2.5	6.48	9.17
220	2.3	6.26	8.85

Table 1. Noise levels for a CMB stage IV experiment in different bands. The total noise contribution is the inverse weighted sum of the individual noise contributions in each band.

To solve the system of linearized Einstein and fluid equations, we use the publicly available Boltzmann solver CLASS [74].

An example of how the ALP isocurvature perturbations generated after inflation affect CMB anisotropies and the linear matter power spectrum (in comoving gauge) is depicted in figure 2. The resulting spectra corresponding to adiabatic and isocurvature modes are shown as solid and dashed lines, respectively. Since the two modes are assumed to be uncorrelated for ALP DM, the total spectra are given by the sum of the individual ones. Generally, the imprint of isocurvature perturbations becomes more prominent with decreasing scale. For low-redshift observations such as galaxy surveys, nonlinearities in the gravitational interaction are already important for $k \gtrsim 0.01h \text{ Mpc}^{-1}$, which complicates the interpretation of measurements and, most likely, dilutes the ALP signal. However, probes of the matter power spectrum at higher redshifts (e.g., during the epoch of reionization), where gravitational nonlinearities are much less developed, could provide interesting bounds on f_{iso} in addition to CMB observations.

3.2 CMB experiments

Forecasts. The main CMB observables are the temperature (T) and polarization fluctuations (E - and B -mode polarization) which emerge from the potential landscape and the anisotropy of Thomson scattering at the surface of last scattering, respectively. In what follows, we do not consider secondary anisotropies such as the Sunyaev-Zeldovich effect [75] or CMB lensing [e.g., 76] and the integrated Sachs-Wolfe effect [77]. Accordingly, we assume to have foreground-cleansed maps of the CMB that can be decomposed into spherical harmonics with coefficients

$$\hat{a}_{\ell m}^X = a_{\ell m}^X + n_{\ell m}^X, \quad (3.7)$$

where $a_{\ell m}^X$ denotes the signal, $n_{\ell m}^X$ the noise, and $X = T, E$ labels the corresponding probe. Here we ignore B -modes as an additional probe since they only give rise to a tiny signal in the simplest inflationary scenarios and are primarily generated by CMB lensing. For Gaussian random fields, all statistical properties are encoded in the two-point correlation function, $C_\ell^{XY} = \langle a_{\ell m}^X a_{\ell m}^{Y*} \rangle$. To model the instrumental noise, we adopt the functional form

$$N_\ell^{XX} = \sigma_X^2 \exp \left[\ell(\ell + 1) \frac{\theta_{\text{beam}}^2}{8 \log 2} \right], \quad (3.8)$$

where θ_{beam} is the beam width and σ_X^2 is the noise of the measurement. The expected noise specifications for CMB stage IV (s4) experiments [56] are summarized in table 1.

Assuming Gaussian data and combining the information from all multipoles, the likelihood can be written as

$$p(\{\mathbf{a}_{\ell m}\}|\boldsymbol{\theta}) = \prod_{\ell} \left[\frac{1}{\sqrt{(2\pi)^2 \det \mathbf{C}}} \exp\left(\mathbf{a}_{\ell m}^{\dagger} \mathbf{C}^{-1} \mathbf{a}_{\ell m}\right) \right]^{2\ell+1}, \quad (3.9)$$

where the $a_{\ell m}^X$ are assumed to be statistically independent. To obtain forecasts, it suffices to adopt the likelihood as given in eq. (3.9) from which the Fisher information matrix is readily obtained as [73]

$$F_{ij}(\boldsymbol{\theta}) = \sum_{\ell} \frac{2\ell+1}{2} \text{tr} \left[\hat{\mathbf{C}}^{-1} \partial_i \hat{\mathbf{C}} \hat{\mathbf{C}}^{-1} \partial_j \hat{\mathbf{C}} \right]_{\boldsymbol{\theta}}, \quad (3.10)$$

where hats indicate the inclusion of noise according to eq. (3.7), and ∂_i denotes the derivative with respect to the i -th parameter $\boldsymbol{\theta}_i$. Partial sky coverage of the data is taken into account by multiplying eq. (3.10) with the sky fraction f_{sky} . For CMB stage III (s3) experiments, we collect multipoles within the range $\ell = 30$ –2500, which is extended to $\ell = 5000$ in both polarization and temperature for a CMB s4 survey. In both cases, the sky fraction is assumed as $f_{\text{sky}} = 0.7$.

Planck data. Additionally, we fit the above model to the 2015 Planck data release [54] for which the likelihoods are publicly available. Compared to the latest data release [78], we note only slight changes in the overall constraints on cosmological parameters. We use the *Planck lite* likelihood which fits the TT power spectrum in the multipole range $\ell = 30$ –2508. *Planck lite* is a pre-marginalized version of the TT likelihood where all nuisance parameters (modulo Planck’s absolute calibration) have been marginalized over prior to sampling. This choice speeds up the analysis dramatically since the number of nuisance parameters is reduced to just one. To sample from the likelihood, we use MONTEPYTHON [79] which is interfaced with CLASS and sampling techniques such as MULTINEST [80, 81] and COSMOHAMMER [82] embedding EMCEE [83, 84].

3.3 HI intensity mapping

Next-generation radio telescopes such as the SKA [57–59] are capable of probing fluctuations in the brightness temperature of the 21-cm neutral hydrogen line during the epoch of reionization with high sensitivity. At redshifts well before reionization is complete, the power spectrum of these fluctuations should provide a close tracer of the underlying matter power spectrum and its measurement offers cosmological constraints that are complementary to CMB and galaxy clustering observations. Reliably extracting the cosmological information from the 21-cm signal will be challenging due to foreground contaminants and other astrophysical complexities, and it is presently unknown how well these systematics will be under control [85, 86]. To estimate future 21-cm constraints on a possible ALP isocurvature mode, we focus on statistical uncertainties and consider an optimistic scenario where density fluctuations dominate the observed signal and all relevant astrophysical effects (including biases of the density field) can be accurately modeled or removed.

Assuming an average neutral hydrogen fraction $\bar{x}_H \approx 1$ and a spin temperature $T_S \gg T_{\text{CMB}}$, fluctuations in the 21-cm brightness temperature relative to the CMB at position \mathbf{r} can be expressed as [e.g., 87, 88]

$$\delta_{21}(\mathbf{r}) = \frac{\Delta T_{21}(\mathbf{r})}{T_0} \approx \bar{x}_H \delta(\mathbf{r}), \quad (3.11)$$

where effects due to peculiar velocities have been neglected, δ is the matter density contrast, and T_0 denotes the average brightness temperature for $\bar{x}_H = 1$ and an observed (redshifted) frequency $\nu = R\nu_0 \approx 1420/(1+z)$ MHz [88],

$$T_0 \approx 26 \frac{\Omega_b h^2}{0.022} \left(\frac{0.15}{\Omega_m h^2} \frac{1+z}{10} \right)^{1/2} \text{ mK}. \quad (3.12)$$

Using eq. (3.11), the corresponding power spectra are simply related by $P_{21} \approx \bar{x}_H^2 P_{\delta\delta}$. The expected error on measurements of $P_{21}(k, \mu)$ for a single field at frequency $\nu = c/\lambda$ is given by a combination of cosmic variance and instrumental noise [89, 90],

$$\sigma_{21}^2(k, \mu) = \left[P_{21}(k, \mu) + \frac{T_{\text{sys}}^2}{T_0^2} \frac{D^2 \Delta D}{B t_{\text{int}} n(k_\perp)} \left(\frac{\lambda^2}{A_e} \right)^2 \right]^2, \quad (3.13)$$

where μ is defined such that $k_\parallel = \mu k$ and $k^2 = k_\perp^2 + k_\parallel^2$ (only modes in the upper half-plane are considered). Here T_{sys} describes the system temperature, $D(z)$ is the comoving distance to the survey volume, ΔD denotes the survey depth, B is the bandwidth, and t_{int} is the total observation time. The effective collecting area per antenna tile, A_e , and the baseline density, $n(k_\perp)$, depend on instrumentation and array design. The error on the spherically averaged power spectrum can be obtained from

$$\frac{1}{\sigma_{21}^2(k)} = \sum_\mu \frac{k^2 \Delta k V_s}{4\pi^2} \frac{\Delta\mu}{\sigma_{21}^2(k, \mu)}, \quad \mu > 0, \quad (3.14)$$

where we choose a bin width $\Delta k = 0.5k$ and $V_s = D^2 \Delta D \lambda^2 / A_e$ is the effective survey volume. For our calculations, we approximate the sum in eq. (3.14) by an integral.

Assuming that T_{sys} is set by the sky temperature, we take $T_{\text{sys}} \approx 280[(1+z)/7.5]^{2.3}$ K [91]. In addition, we fix $B = 8$ MHz to ensure a sufficiently small signal variation over the corresponding redshift range. The depth ΔD depends on B and may be estimated from

$$\Delta D \approx \frac{c(1+z)^2 B}{\nu_0 H(z)} \approx 1.7 \left(\frac{B}{0.1 \text{ MHz}} \right) \left(\frac{1+z}{10} \right)^{1/2} \left(\frac{\Omega_m h^2}{0.15} \right)^{-1/2} \text{ Mpc}. \quad (3.15)$$

For an SKA-like survey, we further adopt $A_e \approx 290 \min[\lambda^2/3, 3.2 \text{ m}^2]$, yielding $A_e(z=8) \approx 350 \text{ m}^2$ and $A_e(z \gtrsim 14) \approx 925 \text{ m}^2$ [92]. In the continuous approximation, $n(k_\perp)$ follows from a convolution of the antenna configuration. For simplicity, we assume a circularly symmetric array with constant baseline density up to a maximum baseline r_{max} ,

$$n(|\mathbf{u}|) = \frac{\lambda^2 N_a (N_a - 1)}{\pi r_{\text{max}}^2} \approx \frac{\lambda^2 N_a^2}{\pi r_{\text{max}}^2}, \quad \lambda |\mathbf{u}| < r_{\text{max}}, \quad (3.16)$$

and zero otherwise, where \mathbf{u} is the dimensionless baseline vector in visibility space, satisfying $|\mathbf{u}| = k_\perp D(z)/2\pi$, and N_a is the total number of antennae. Setting $r_{\text{max}} = 1$ km, we obtain an average sensitivity ~ 0.9 , which is in good agreement with typically adopted specifications [92, 93]. The discrete nature of the array configuration prohibits measurements for arbitrarily small baselines. For an SKA-like survey, we choose a minimum baseline $r_{\text{min}} = 35$ m.

Below we will consider two different stages of an SKA-like experiment. For an idealized SKA1 setup targeting redshifts $z \gtrsim 6$, we take $N_a = 900$, and we assume that this number

Experiment	f_{iso}	α_s	$\sum m_\nu [\text{eV}]$	n_s	A_s	Ω_b	τ	h	Ω_m	\bar{x}_H
s3	0.38	0.0052	0.34	0.0034	0.021	0.0045	0.0045	0.032	0.038	-
s3+SKA1	0.20	0.0044	0.28	0.0031	0.021	0.0037	0.0043	0.027	0.031	0.082
s4	0.067	0.0018	0.050	0.0016	0.0080	0.00064	0.0017	0.0045	0.0053	-
s4+SKA2	0.016	0.0017	0.042	0.0016	0.0080	0.00051	0.0017	0.0034	0.0040	0.012

Table 2. Parameters used in the Fisher forecasts outlined in sections 3.2 and 3.3. Shown are the marginalized 1σ -errors of each parameter for the experiment(s) given in the first column. For both SKA1 and SKA2, we assume single-field observations at $z = 8$ and $t_{\text{int}} = 2000$ h. As described in the text, the reference model adopts $\bar{x}_H = 1$ and $f_{\text{iso}} = 0.005$, other fiducial values are summarized at the end of section 1.

further increases to $N_a = 3600$ in an SKA2 phase [92]. To account for foregrounds, we follow previous works [e.g., 88, 90] by imposing a lower bound on the observable wavelengths. The cleaning process relies on the expectation that foregrounds are spectrally smooth, whereas the signal has structure in frequency space. At the very least, this will remove all line-of-sight modes with $k_{\parallel} \leq 2\pi/\Delta D$. From the discreteness of modes in the survey it then follows that all modes satisfying

$$k \leq 2\pi/\Delta D \quad (3.17)$$

will be lost. Considering a fiducial survey volume at $z \sim 8$ and restricting the analysis to linear modes, significant constraints on the matter power spectrum are typically obtained for $k \sim 0.1\text{--}1h \text{ Mpc}^{-1}$. Concerning the computation of the Fisher matrix, we assume measurements in seven non-overlapping bins covering the range $k \approx 0.08\text{--}2.7h \text{ Mpc}^{-1}$, with Δk as specified above. Since the CMB probes the power spectrum at much larger scales, the corresponding likelihoods may simply be added to arrive at combined forecasts.

4 Results

In this section, we discuss forecasts on constraints from CMB anisotropies and HI intensity mapping on the isocurvature amplitude, as well as bounds based on current Planck data (section 4.1). These are then converted into constraints on ALP masses (section 4.2). Regarding our analysis, we will adopt two cosmological models, one for the Fisher forecasts specified by a total of ten parameters (listed in table 2), and a standard flat six-parameter cosmological model (Λ CDM) extended by f_{iso} and used to fit the Planck likelihood described in section 3.2.

4.1 Bounds on the isocurvature amplitude

Concerning forecasts based on the Fisher matrix formalism, we consider the set of parameters presented in table 2. In particular, these refer to the spectral index of the primordial power spectrum, n_s , its running α_s and amplitude A_s (defined at the pivot scale $k_* = 0.05 \text{ Mpc}^{-1}$), the sum of neutrino masses $\sum m_\nu$, the Hubble constant $H_0 = 100h \text{ km s}^{-1} \text{ Mpc}^{-1}$ expressed in terms of the dimensionless Hubble parameter h , the optical depth τ , and the baryon and total matter density parameters Ω_b and Ω_m , respectively. Further, f_{iso} describes the relative amplitude of isocurvature fluctuations as defined in eq. (3.6), and \bar{x}_H is the neutral hydrogen fraction that enters in the analysis of 21-cm experiments discussed in section 3.3. Note that the ALP DM density parameter Ω_a in presence of neutrinos is given by

$$\Omega_a \equiv \Omega_m - \Omega_b - \frac{\sum m_\nu}{93.14h^2}. \quad (4.1)$$

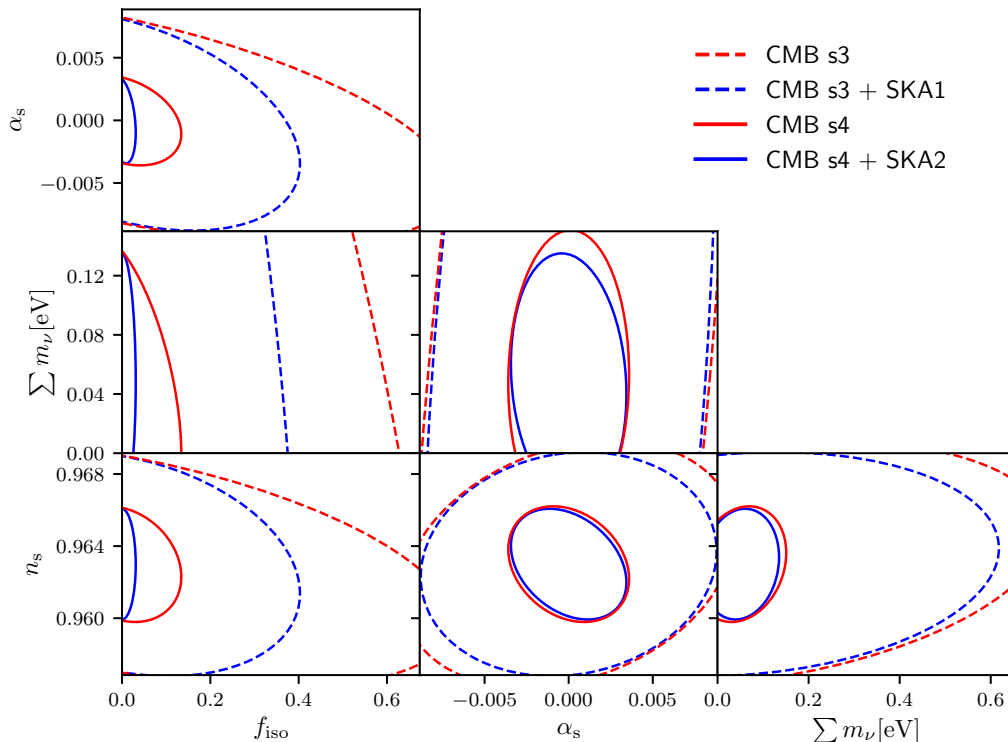


Figure 3. Marginalized 1σ -contours for the parameters f_{iso} , n_s , α_s , and $\sum m_\nu$ obtained from the Fisher analysis, assuming the parameters listed in [table 2](#). Dashed contours indicate results for CMB s3 surveys while solid curves correspond to future s4 experiments. Red curves show constraints based on CMB observations alone, blue curves refer to combinations with HI intensity mapping experiments. For both SKA1 and SKA2, we assume single-field observations at $z = 8$ and $t_{\text{int}} = 2000$ h.

For our reference model, we set $\bar{x}_H = 1$ and $f_{\text{iso}} = 0.005$. The small, but non-zero value of f_{iso} is chosen to avoid numerical issues in the computation of the Fisher matrix and should be understood as a proxy for a vanishing isocurvature component. The fiducial values of all remaining cosmological parameters can be found at the end of [section 1](#).

Focusing on the parameters f_{iso} , n_s , α_s , and $\sum m_\nu$, [figure 3](#) shows the resulting marginalized 1σ -contours for CMB s3 and s4 experiments as well as for their combination with the idealized 21-cm surveys from [section 3.3](#). For both SKA1 and SKA2, we assume single-field observations at $z = 8$ and a total observation time $t_{\text{int}} = 2000$ h, which roughly translates into a 2-year measurement period. The corresponding 1σ -constraints for all parameters and the same combinations of experiments are summarized in [table 2](#). From the figure, we clearly see that the constraints on f_{iso} are greatly improved when considering a CMB s4 experiment alone. This is in large part due to the drastically increased sensitivity of these experiments in polarization measurements. Also, the general trend of tighter bounds from future surveys can be understood from their improved ability to probe higher wave numbers where the imprint of the ALP isocurvature mode becomes more pronounced (see [section 3.1](#)). As we will discuss in the context of Planck data below, the condition $f_{\text{iso}} \geq 0$ hampers a straightforward

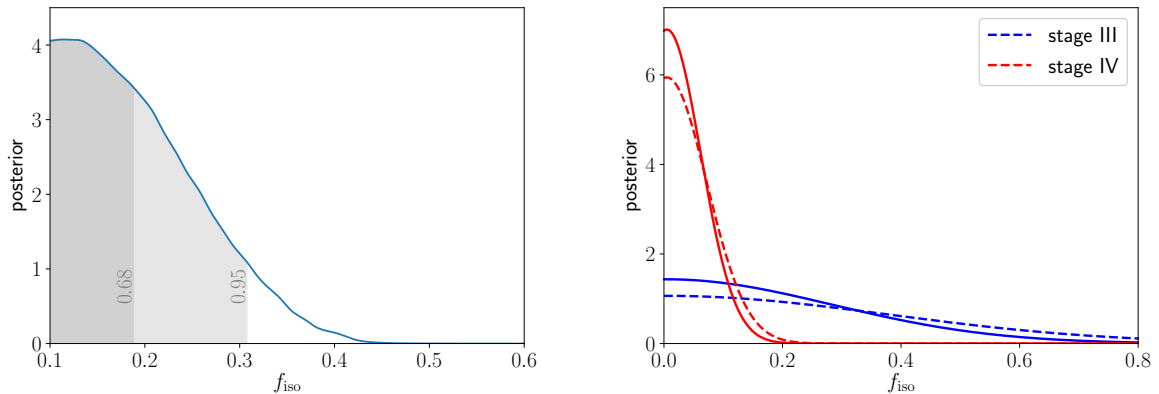


Figure 4. Posterior distribution of the isocurvature amplitude f_{iso} . The left panel illustrates the posterior distribution from *Planck_lite* including corresponding confidence regions. The right panel shows the effect of marginalizing over α_s and $\sum m_\nu$ on CMB forecasts. Dashed curves indicate the posterior after marginalizing over the full cosmology as summarized in table 2. Solid curves show the posterior when both α_s and $\sum m_\nu$ are kept fixed.

interpretation of the inferred f_{iso} -errors from the Fisher analysis in terms of usual confidence intervals. Therefore, the quoted uncertainties on f_{iso} should be taken as rough estimates.

Looking at figure 3, we further notice degeneracies between f_{iso} and other parameters that determine the shape of the matter power spectrum. While the resulting degeneracy with the sum of neutrino masses appears to be very weak, it is found to be quite appreciable for the two shape parameters n_s and α_s . Interestingly, combining CMB observations with HI intensity mapping experiments can break these degeneracies to some extent. In general, we see that the addition of 21-cm observations significantly tightens the constraints on f_{iso} . Considering our estimates for the SKA2 survey, the bound is reduced by another factor of 5 compared to a pure CMB experiment, resulting in the limit $f_{\text{iso}} \leq 0.016$. Other constraints could come from even smaller scales or, for instance, from weak lensing analyses. However, this would require a thorough understanding of the evolution of isocurvature fluctuations on scales that are already in the nonlinear regime of structure formation.

Finally, we study constraints on f_{iso} based on the Planck 2015 data. To this end, we fit a standard 6-parameter Λ CDM model extended by f_{iso} to the temperature power spectrum as described in section 3.2. The results are presented in the left panel of figure 4 where we plot the marginalized posterior distribution of f_{iso} . It is found that Planck yields a 2σ -bound of $f_{\text{iso}} \leq 0.31$. In the right panel of figure 4, we illustrate the impact of reducing the model's parameter space in the Planck data analysis. Omitting the spectral running, α_s , and the sum of the neutrino masses, $\sum m_\nu$, tightens the posterior slightly and leads to a small improvement of the constraints. A few comments on these two plots are in order. The constraints from Planck outperform the CMB s3 forecast even if α_s and $\sum m_\nu$ are not marginalized over. The reason for this is that we evaluate the Fisher matrix in a region where the curvature of the log-likelihood is relatively small since f_{iso} is bounded by zero. Therefore, the actual posterior distribution is very asymmetric and turns very flat towards zero. Hence, the constraints derived from the Fisher matrix turn out weaker. Note that the addition of the E -mode spectrum in the forecasts, which is not included in the *Planck_lite* likelihood, yields only small changes in the constraints due to the high noise levels assumed for CMB s3

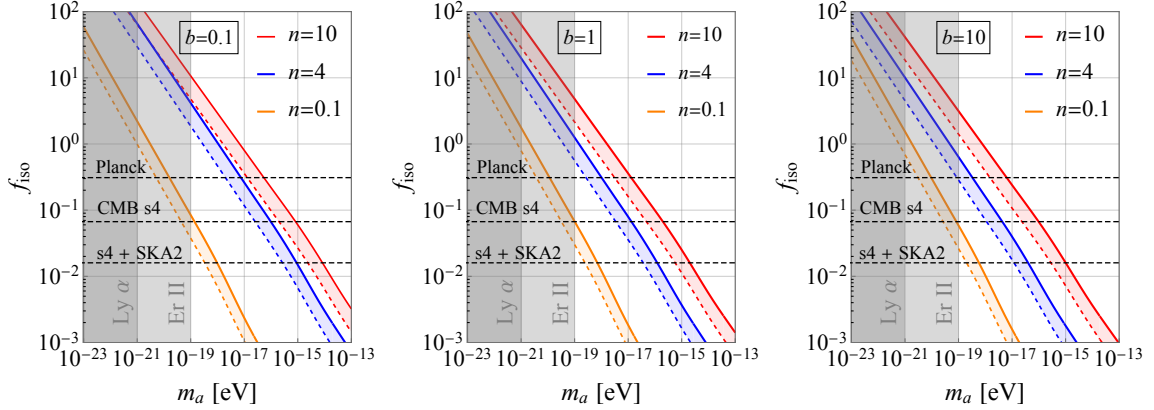


Figure 5. Predicted isocurvature fraction according to eq. (4.2) as a function of the zero-temperature ALP mass m_a for different assumptions on the ALP mass-temperature dependence parametrized by n and b as defined in eq. (2.2). Solid curves correspond to our estimate of the isocurvature amplitude, and bands between solid and dashed curves indicate a factor 5 uncertainty. Horizontal dotted lines show upper bounds on f_{iso} from Planck (2σ -level) and the sensitivity of future CMB s4 and advanced 21-cm experiments (SKA2). Shaded regions correspond to those of figure 1. The PQ breaking scale f_a is fixed for each m_a by requiring that ALPs provide all DM.

polarization measurements.

It is interesting to compare our results to the isocurvature bounds obtained by the Planck collaboration [46, 94]. Their analysis uses different models to constrain the isocurvature component. The most general one assumes a free power law for the isocurvature, adiabatic and cross fluctuations. The power law is constructed between $k = 0.002\text{--}0.1 \text{ Mpc}^{-1}$, i.e. over scales accessible to Planck. For these models, it is found that $\beta \leq 0.37$ at $k_* = 0.05 \text{ Mpc}^{-1}$, where $\beta \equiv f_{\text{iso}}^2 / (1 + f_{\text{iso}}^2)$. Our bound $f_{\text{iso}} \leq 0.31$ corresponds to $\beta \leq 0.088$. Since the model presented here consists of fewer parameter (in particular, the slope of the isocurvature power spectrum is fixed by the ALP model), these estimates appear consistent with each other. A specific axion model with fixed primordial tilt (spectral index) $n_s^{\text{iso}} = 1$ and free amplitude is considered in [94], leading to $\beta \lesssim 0.04$. This model, however, requires PQ symmetry breaking before the end of inflation, in contrast to our assumption. Similarly, axion models with free spectral tilt [46] cannot be directly compared to our case (where $n_s^{\text{iso}} = 4$ is fixed).

4.2 Implications for ALP masses

Using our prediction for the ALP isocurvature power spectrum eq. (2.17) and the parametrization of the adiabatic spectrum in eq. (3.3), we can relate the value of f_{iso} to the underlying ALP parameters,

$$f_{\text{iso}} = \sqrt{\frac{C k_*^3}{A_s K^3}}, \quad (4.2)$$

where the values of C and K are calculated as described in section 2. Assuming the fiducial value $A_s = 2.215 \times 10^{-9}$, we see that the isocurvature fraction on CMB scales becomes of order one for $K/k_* \sim (A_s/C)^{-1/3} \sim 1000$.

In figure 5, we show the predicted values of f_{iso} as a function of the ALP mass m_a for different assumptions on the mass-temperature dependence $m_a(T)$. The width of the bands

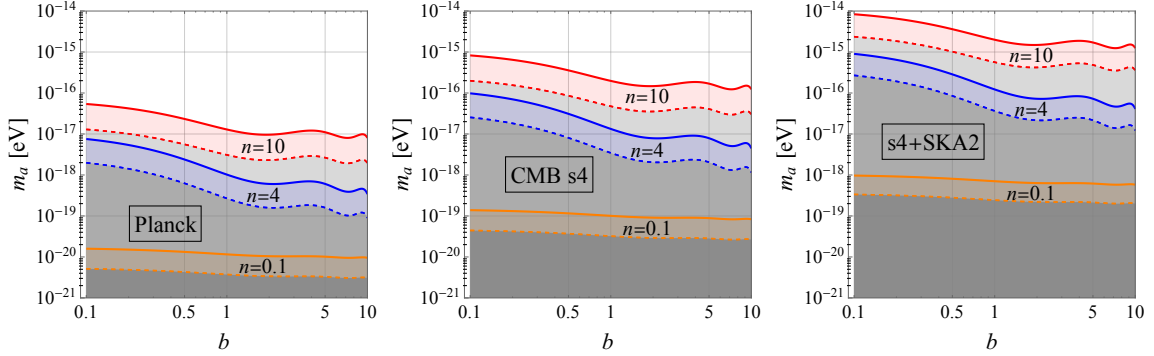


Figure 6. Constraints on the zero-temperature ALP mass m_a from isocurvature fluctuations for different assumptions on the mass-temperature dependence by n and b as defined in eq. (2.2). ALPs are assumed to provide all DM. Solid curves correspond to our estimate of the isocurvature amplitude, and bands between solid and dashed curves indicate a factor 5 uncertainty. The left panel corresponds to $f_{\text{iso}} < 0.31$ (2σ -level) from Planck. The middle and right panels show, respectively, potential bounds assuming 1σ -sensitivities of a future CMB s4 experiment ($f_{\text{iso}} < 0.067$) and its combination with an SKA2-like 21-cm survey ($f_{\text{iso}} < 0.016$). The region below the curves is disfavoured.

indicates a factor 5 systematic uncertainty in predicting the amplitude, i.e. the constant C in eq. (4.2), as we discussed in section 2.4. The qualitative behaviour of these curves follows from the K -dependence shown in the right panel of figure 1 since, up to a minor dependence on C , we roughly have $f_{\text{iso}} \propto K^{-3/2}$ from eq. (4.2). From the estimates in section 2.1, we, therefore, expect that $f_{\text{iso}} \propto m_a^{-3/4}$ ($m_a^{-1/2}$) in the small- n (large- n) limit, in good agreement with the figure.

For $m_a \lesssim 10^{-16}$ eV, we observe from figure 5 that the amplitude of isocurvature fluctuations with $k \sim k_*$ can become comparable to the adiabatic modes and, therefore, relevant to CMB observations. The predicted values of f_{iso} are compared to the CMB bounds implied by Planck, as well as the sensitivity of future CMB s4 and 21-cm experiments. In the regions of parameter space where, the predictions for f_{iso} exceed the Planck constraint $f_{\text{iso}} < 0.31$, the assumption of post-inflationary ALP DM is excluded at the 2σ -level. This excluded region is illustrated in the left panel of figure 6. The exclusion is stronger for large values of n and small values of b . For $n = 10$, we see that values of $m_a \lesssim 10^{-17}$ eV are excluded. Even in the small n -limit, the non-trivial exclusion for $m_a \lesssim 10^{-20}$ eV is obtained, somewhat stronger than constraints obtained from the Lyman- α forest [41, 42]. Note that our bounds on ULAs extend to much larger masses than the ones obtained from CMB and large-scale structure data in [36–40], but rely on the post-inflationary hypothesis.

The middle panel of figure 6 shows the potential improvement corresponding to a sensitivity $f_{\text{iso}} < 0.067$ (1σ -level) for a future CMB s4 experiment. We observe that the exclusion limits on m_a become roughly one order of magnitude stronger. Finally, the right panel corresponds to the limit $f_{\text{iso}} < 0.016$ (1σ -level), potentially achievable with the combination of CMB s4 experiments and advanced 21-cm observations based on an optimistic SKA2 configuration, which would lead to another order of magnitude improvement in m_a . In the most optimistic case, a limit of $m_a \gtrsim 10^{-14}$ eV could be achieved while a more robust bound (with respect to the mass-temperature dependence) is $m_a \gtrsim \text{few} \times 10^{-19}$ eV.

5 Discussion and conclusion

In this paper, we investigated mass bounds on ALP dark matter derived from observations of the large-scale structure of the Universe. If the PQ symmetry is broken after inflation, additional isocurvature fluctuations are generated on top of the adiabatic spectrum. These isocurvature fluctuations have a white noise power spectrum, with a cutoff corresponding to the size of the horizon at the time when the ALP field starts to oscillate. By requiring that the ALPs provide all DM, we derived the amplitude of the isocurvature fluctuations relative to the adiabatic component as a function of the ALP model parameters. In our analysis, we used the following model assumptions:

- a) We assume a two-parameter model for the mass-temperature dependence of ALPs given by a power law with index n , and a parameter b that determines the temperature at which the zero-temperature mass is reached.
- b) We use the harmonic approximation of the ALP potential and assume that the DM energy density is generated by the realignment mechanism. This introduces uncertainties in our calculation of the DM density and the amplitude of isocurvature fluctuations. However, the overall uncertainties are dominated by the ALP model dependence in assumption *a*).
- c) The PQ symmetry is broken after the end of inflation. For very small ALP masses, this requires relatively high values of the energy scale of inflation. Generically, this could give rise to tensor-to-scalar ratios in the observable range. A more thorough discussion of this condition is presented in [section 2.4](#).
- d) The cosmological evolution of ALPs can effectively be treated as cold DM and the imprint on large-scale structure is determined by their initial power spectrum. For the ALP mass range and the cosmological scales considered here, this assumption is well justified.

With these assumptions, we were able to derive constraints on the ALP mass for different models of the mass-temperature dependence. In particular, we focused on observations probing linear scales given by CMB and HI intensity mapping experiments. Our findings are the following:

- i) CMB observations by the Planck satellite set a lower bound on the ALP mass ranging from 10^{-20} eV for very shallow mass dependences to 10^{-16} eV for very steep ones. The limits are generally tighter for small values of b .
- ii) CMB s4 experiments will improve these limits by roughly one order of magnitude due to the increased sensitivity in polarization measurements at high multipoles.
- iii) Adding HI intensity mapping in the form of an SKA2-like experiment could further boost these limits by an additional order of magnitude, providing a limit of $m_a \geq 10^{-14}$ eV in the most optimistic scenario.

Our results are complementary to other works [[36–42](#)]. Typically, our derived limits are stronger, but rely on the assumptions summarized above (in particular, the post-inflationary scenario). While isocurvature constraints are already well established in the pre-inflationary axion scenario, our analysis has shown that also in the post-inflationary case, isocurvature fluctuations are a robust prediction of ALP DM models and lead to powerful constraints.

Note that our results are based only on gravitational effects and do not require assumptions about possible couplings to photons.

Concerning assumption b), let us mention that including the full ALP potential will give rise to an additional production mechanism from cosmic strings. This may change the energy density and the amplitude of isocurvature fluctuations by factors of order unity. However, it is expected that the main feature of the scenario, namely a white noise isocurvature power spectrum at large distance scales, is a robust prediction.

Important questions in the future concern the cosmological evolution of miniclusters, especially in the nonlinear regime of structure formation and for scales and masses where they cannot necessarily be treated as cold DM. While the observations considered here focused on linear scales, nonlinear scales might provide an additional rich phenomenology for ALPs.

Acknowledgments

This research was supported by the Excellence Initiative of the German Federal and State Governments at Heidelberg University, by the European Union's Horizon 2020 research and innovation programme under the Marie Skłodowska-Curie grant agreement No 674896 (Elusives), and by the Heidelberg Karlsruhe Research Partnership (HEiKA).

References

- [1] G. Bertone, D. Hooper and J. Silk, *Particle dark matter: evidence, candidates and constraints*, *Phys. Rep.* **405** (2005) 279 [[hep-ph/0404175](#)].
- [2] G. Bertone and D. Hooper, *History of dark matter*, *Rev. Mod. Phys.* **90** (2018) 045002 [[1605.04909](#)].
- [3] A. G. Riess, A. V. Filippenko, P. Challis and et al., *Observational Evidence from Supernovae for an Accelerating Universe and a Cosmological Constant*, *Astron. J.* **116** (1998) 1009.
- [4] S. Perlmutter, G. Aldering, G. Goldhaber and et al., *Measurements of Omega and Lambda from 42 High-Redshift Supernovae*, *Astrophys. J.* **517** (1999) 565.
- [5] Planck Collaboration, P. A. R. Ade, N. Aghanim, M. Arnaud, M. Ashdown, J. Aumont et al., *Planck 2015 results. XIII. Cosmological parameters*, *Astron. Astrophys.* **594** (2016) A13.
- [6] M. Bartelmann, *The dark Universe*, *Rev. Mod. Phys.* **82** (2010) 331 [[0906.5036](#)].
- [7] F. Zwicky, *Die Rotverschiebung von extragalaktischen Nebeln*, *Helv. Phys. Acta* **6** (1933) 110.
- [8] S. Smith, *The Mass of the Virgo Cluster*, *Astrophys. J.* **83** (1936) 23.
- [9] S. Weinberg, *A New Light Boson?*, *Phys. Rev. Lett.* **40** (1978) 223.
- [10] F. Wilczek, *Problem of Strong P and T Invariance in the Presence of Instantons*, *Phys. Rev. Lett.* **40** (1978) 279.
- [11] P. Sikivie, *Axion Cosmology*, *Lect. Notes Phys.* **741** (2008) 19 [[astro-ph/0610440](#)].
- [12] D. J. E. Marsh, *Axion Cosmology*, *Phys. Rep.* **643** (2016) 1 [[1510.07633](#)].
- [13] R. D. Peccei and H. R. Quinn, *CP Conservation in the Presence of Instantons*, *Phys. Rev. Lett.* **38** (1977) 1440.
- [14] M. Dine, W. Fischler and M. Srednicki, *A simple solution to the strong cp problem with a harmless axion*, *Phys. Lett. B* **104** (1981) 199 .
- [15] A. R. Zhitnitsky, *On Possible Suppression of the Axion Hadron Interactions. (In Russian)*, *Sov. J. Nucl. Phys.* **31** (1980) 260.

- [16] J. E. Kim, *Weak-interaction singlet and strong CP invariance*, *Phys. Rev. Lett.* **43** (1979) 103.
- [17] M. Shifman, A. Vainshtein and V. Zakharov, *Can confinement ensure natural cp invariance of strong interactions?*, *Nucl. Phys. B* **166** (1980) 493 .
- [18] A. Arvanitaki, S. Dimopoulos, S. Dubovsky, N. Kaloper and J. March-Russell, *String Axiverse*, *Phys. Rev. D* **81** (2010) 123530 [[0905.4720](#)].
- [19] P. Arias, D. Cadamuro, M. Goodsell, J. Jaeckel, J. Redondo and A. Ringwald, *WISPy Cold Dark Matter*, *J. Cosmol. Astropart. Phys.* **1206** (2012) 013 [[1201.5902](#)].
- [20] A. Ringwald, *Exploring the Role of Axions and Other WISPs in the Dark Universe*, *Phys. Dark Univ.* **1** (2012) 116 [[1210.5081](#)].
- [21] M. Dine and W. Fischler, *The Not So Harmless Axion*, *Phys. Lett. B* **120** (1983) 137.
- [22] J. Preskill, M. B. Wise and F. Wilczek, *Cosmology of the Invisible Axion*, *Phys. Lett. B* **120** (1983) 127.
- [23] M. S. Turner, *Coherent Scalar Field Oscillations in an Expanding Universe*, *Phys. Rev. D* **28** (1983) 1243.
- [24] L. F. Abbott and P. Sikivie, *A Cosmological Bound on the Invisible Axion*, *Phys. Lett. B* **120** (1983) 133.
- [25] L. Visinelli and P. Gondolo, *Dark matter axions revisited*, *Phys. Rev. D* **80** (2009) 035024.
- [26] M. Kawasaki, K. Saikawa and T. Sekiguchi, *Axion dark matter from topological defects*, *Phys. Rev. D* **91** (2015) 065014 [[1412.0789](#)].
- [27] V. B. Klaer and G. D. Moore, *The dark-matter axion mass*, *J. Cosmol. Astropart. Phys.* **1711** (2017) 049 [[1708.07521](#)].
- [28] C. J. Hogan and M. J. Rees, *Axion miniclusters*, *Phys. Lett. B* **205** (1988) 228.
- [29] E. W. Kolb and I. I. Tkachev, *Axion miniclusters and Bose stars*, *Phys. Rev. Lett.* **71** (1993) 3051 [[hep-ph/9303313](#)].
- [30] E. W. Kolb and I. I. Tkachev, *Nonlinear axion dynamics and formation of cosmological pseudosolitons*, *Phys. Rev. D* **49** (1994) 5040 [[astro-ph/9311037](#)].
- [31] E. W. Kolb and I. I. Tkachev, *Femtolensing and picolensing by axion miniclusters*, *Astrophys. J.* **460** (1996) L25 [[astro-ph/9510043](#)].
- [32] K. M. Zurek, C. J. Hogan and T. R. Quinn, *Astrophysical Effects of Scalar Dark Matter Miniclusters*, *Phys. Rev. D* **75** (2007) 043511 [[astro-ph/0607341](#)].
- [33] E. Hardy, *Miniclusters in the Axiverse*, *J. High Energy Phys.* **02** (2017) 046 [[1609.00208](#)].
- [34] J. Enander, A. Pargner and T. Schwetz, *Axion minicluster power spectrum and mass function*, *J. Cosmol. Astropart. Phys.* **1712** (2017) 038 [[1708.04466](#)].
- [35] A. Vaquero, J. Redondo and J. Stadler, *Early seeds of of axion miniclusters*, [1809.09241](#).
- [36] L. Amendola and R. Barbieri, *Dark matter from an ultra-light pseudo-Goldstone-boson*, *Phys. Lett. B* **642** (2006) 192 [[hep-ph/0509257](#)].
- [37] D. J. E. Marsh and P. G. Ferreira, *Ultra-Light Scalar Fields and the Growth of Structure in the Universe*, *Phys. Rev. D* **82** (2010) 103528 [[1009.3501](#)].
- [38] D. J. E. Marsh, E. Macaulay, M. Trebitsch and P. G. Ferreira, *Ultra-light Axions: Degeneracies with Massive Neutrinos and Forecasts for Future Cosmological Observations*, *Phys. Rev. D* **85** (2012) 103514 [[1110.0502](#)].
- [39] R. Hlozek, D. Grin, D. J. E. Marsh and P. G. Ferreira, *A search for ultralight axions using precision cosmological data*, *Phys. Rev. D* **91** (2015) 103512 [[1410.2896](#)].

- [40] R. Hlozek, D. J. E. Marsh and D. Grin, *Using the Full Power of the Cosmic Microwave Background to Probe Axion Dark Matter*, *Mon. Notices Royal Astron. Soc.* **476** (2018) 3063 [[1708.05681](#)].
- [41] V. Iršič, M. Viel, M. G. Haehnelt, J. S. Bolton and G. D. Becker, *First constraints on fuzzy dark matter from Lyman- α forest data and hydrodynamical simulations*, *Phys. Rev. Lett.* **119** (2017) 031302.
- [42] T. Kobayashi, R. Murgia, A. De Simone, V. Iri and M. Viel, *Lyman- α constraints on ultralight scalar dark matter: Implications for the early and late universe*, *Phys. Rev. D* **96** (2017) 123514 [[1708.00015](#)].
- [43] D. J. E. Marsh and J. C. Niemeyer, *Strong Constraints on Fuzzy Dark Matter from Ultrafaint Dwarf Galaxy Eridanus II*, [1810.08543](#).
- [44] A. Arvanitaki, M. Baryakhtar and X. Huang, *Discovering the QCD Axion with Black Holes and Gravitational Waves*, *Phys. Rev. D* **91** (2015) 084011 [[1411.2263](#)].
- [45] M. J. Stott and D. J. E. Marsh, *Black hole spin constraints on the mass spectrum and number of axionlike fields*, *Phys. Rev. D* **98** (2018) 083006 [[1805.02016](#)].
- [46] Planck Collaboration, Y. Akrami, F. Arroja, M. Ashdown, J. Aumont, C. Baccigalupi et al., *Planck 2018 results. X. Constraints on inflation*, [1807.06211](#).
- [47] M. S. Turner and F. Wilczek, *Inflationary axion cosmology*, *Phys. Rev. Lett.* **66** (1991) 5.
- [48] D. H. Lyth, *Axions and inflation: Sitting in the vacuum*, *Phys. Rev. D* **45** (1992) 3394.
- [49] M. Beltran, J. Garcia-Bellido and J. Lesgourgues, *Isocurvature bounds on axions revisited*, *Phys. Rev. D* **75** (2007) 103507 [[hep-ph/0606107](#)].
- [50] M. P. Hertzberg, M. Tegmark and F. Wilczek, *Axion Cosmology and the Energy Scale of Inflation*, *Phys. Rev. D* **78** (2008) 083507 [[0807.1726](#)].
- [51] J. Hamann, S. Hannestad, G. G. Raffelt and Y. Y. Y. Wong, *Isocurvature forecast in the anthropic axion window*, *J. Cosmol. Astropart. Phys.* **0906** (2009) 022 [[0904.0647](#)].
- [52] L. Visinelli, *Light axion-like dark matter must be present during inflation*, *Phys. Rev. D* **96** (2017) 023013 [[1703.08798](#)].
- [53] K. Schmitz and T. T. Yanagida, *Axion Isocurvature Perturbations in Low-Scale Models of Hybrid Inflation*, *Phys. Rev. D* **98** (2018) 075003 [[1806.06056](#)].
- [54] Planck Collaboration, N. Aghanim, M. Arnaud, M. Ashdown, J. Aumont, C. Baccigalupi et al., *Planck 2015 results. XI. CMB power spectra, likelihoods, and robustness of parameters*, *Astron. Astrophys.* **594** (2016) A11 [[1507.02704](#)].
- [55] P. André, C. Baccigalupi, A. Banday, D. Barbosa, B. Barreiro, J. Bartlett et al., *PRISM (Polarized Radiation Imaging and Spectroscopy Mission): an extended white paper*, *J. Cosmol. Astropart. Phys.* **2** (2014) 006 [[1310.1554](#)].
- [56] K. N. Abazajian, P. Adshead, Z. Ahmed, S. W. Allen, D. Alonso, K. S. Arnold et al., *CMB-S4 Science Book, First Edition*, [1610.02743](#).
- [57] Square Kilometre Array Cosmology Science Working Group, R. Maartens, F. B. Abdalla, M. Jarvis and M. G. Santos, *Cosmology with the SKA – overview*, [1501.04076](#).
- [58] Square Kilometre Array Cosmology Science Working Group, D. J. Bacon, R. A. Battye, P. Bull, S. Camera, P. G. Ferreira et al., *Cosmology with Phase 1 of the Square Kilometre Array; Red Book 2018: Technical specifications and performance forecasts*, [1811.02743](#).
- [59] P. Bull, S. Camera, K. Kelley, H. Padmanabhan, J. Pritchard, A. Raccanelli et al., *Fundamental Physics with the Square Kilometer Array*, [1810.02680](#).

- [60] Planck Collaboration, P. A. R. Ade, N. Aghanim, M. Arnaud, M. Ashdown, J. Aumont et al., *Planck 2015 results. XIII. Cosmological parameters*, *Astron. Astrophys.* **594** (2016) A13.
- [61] E. W. Kolb and M. S. Turner, *The early universe*, Frontiers in Physics. Westview Press, Boulder, CO, 1990.
- [62] S. Borsanyi et al., *Calculation of the axion mass based on high-temperature lattice quantum chromodynamics*, *Nature* **539** (2016) 69 [1606.07494].
- [63] G. Grilli di Cortona, E. Hardy, J. Pardo Vega and G. Villadoro, *The QCD axion, precisely*, *J. High Energy Phys.* **01** (2016) 034 [1511.02867].
- [64] T. W. B. Kibble, *Topology of cosmic domains and strings*, *J. Phys. A* **9** (1976) 1387.
- [65] L. Husdal, *On Effective Degrees of Freedom in the Early Universe*, *Galaxies* **4** (2016) 78 [1609.04979].
- [66] M. Gorghetto, E. Hardy and G. Villadoro, *Axions from Strings: the Attractive Solution*, *J. High Energy Phys.* **07** (2018) 151 [1806.04677].
- [67] T. Hiramatsu, M. Kawasaki, K. Saikawa and T. Sekiguchi, *Production of dark matter axions from collapse of string-wall systems*, *Phys. Rev. D* **85** (2012) 105020 [1202.5851].
- [68] M. Kawasaki, T. Sekiguchi, M. Yamaguchi and J. Yokoyama, *Long-term dynamics of cosmological axion strings*, *Prog. Theor. Exp. Phys.* **2018** (2018) 091E01 [1806.05566].
- [69] L. F. Abbott and M. B. Wise, *Constraints on Generalized Inflationary Cosmologies*, *Nucl. Phys. B* **244** (1984) 541.
- [70] A. R. Liddle and D. H. Lyth, *Cosmological Inflation and Large-Scale Structure*. Cambridge Univ. Press, Cambridge, 2000.
- [71] J.-C. Hwang and H. Noh, *Axion as a Cold Dark Matter candidate*, *Phys. Lett. B* **680** (2009) 1 [0902.4738].
- [72] C.-G. Park, J.-C. Hwang and H. Noh, *Axion as a cold dark matter candidate: Low-mass case*, *Phys. Rev. D* **86** (2012) 083535.
- [73] M. Tegmark, A. N. Taylor and A. F. Heavens, *Karhunen-Loeve Eigenvalue Problems in Cosmology: How Should We Tackle Large Data Sets?*, *Astrophys. J.* **480** (1997) 22.
- [74] J. Lesgourgues, *The Cosmic Linear Anisotropy Solving System (CLASS) I: Overview*, [1104.2932](#).
- [75] R. A. Sunyaev and I. B. Zeldovich, *Microwave background radiation as a probe of the contemporary structure and history of the universe*, *Annu. Rev. Astron. Astrophys.* **18** (1980) 537.
- [76] C. M. Hirata and U. Seljak, *Reconstruction of lensing from the cosmic microwave background polarization*, *Phys. Rev. D* **68** (2003) 083002.
- [77] R. K. Sachs and A. M. Wolfe, *Perturbations of a Cosmological Model and Angular Variations of the Microwave Background*, *Astrophys. J.* **147** (1967) 73.
- [78] Planck Collaboration, N. Aghanim, Y. Akrami, M. Ashdown, J. Aumont, C. Baccigalupi et al., *Planck 2018 results. VI. Cosmological parameters*, [1807.06209](#).
- [79] B. Audren, J. Lesgourgues, K. Benabed and S. Prunet, “Monte Python: Monte Carlo code for CLASS in Python.” Astrophysics Source Code Library, July, 2013.
- [80] J. Skilling, *Nested sampling for general bayesian computation*, *Bayesian Anal.* **1** (2006) 833.
- [81] F. Feroz, M. P. Hobson and M. Bridges, “MultiNest: Efficient and Robust Bayesian Inference.” Astrophysics Source Code Library, Sept., 2011.

- [82] J. Akeret, S. Seehars, A. Amara, A. Refregier and A. Csillaghy, *CosmoHammer: Cosmological parameter estimation with the MCMC Hammer*, *Astron. Comput.* **2** (2013) 27.
- [83] J. Goodman and J. Weare, *Ensemble samplers with affine invariance*, *Comm. App. Math. Comp. Sci.* **5** (2010) 65.
- [84] D. Foreman-Mackey, D. W. Hogg, D. Lang and J. Goodman, *emcee: The MCMC Hammer*, *Publ. Astron. Soc. Pac.* **125** (2013) 306 [[1202.3665](#)].
- [85] S. R. Furlanetto, S. P. Oh and F. H. Briggs, *Cosmology at low frequencies: The 21 cm transition and the high-redshift Universe*, *Phys. Rep.* **433** (2006) 181 [[astro-ph/0608032](#)].
- [86] J. R. Pritchard and A. Loeb, *21 cm cosmology in the 21st century*, *Rep. Prog. Phys.* **75** (2012) 086901 [[1109.6012](#)].
- [87] M. Zaldarriaga, S. R. Furlanetto and L. Hernquist, *21 Centimeter Fluctuations from Cosmic Gas at High Redshifts*, *Astrophys. J.* **608** (2004) 622 [[astro-ph/0311514](#)].
- [88] M. McQuinn, O. Zahn, M. Zaldarriaga, L. Hernquist and S. R. Furlanetto, *Cosmological Parameter Estimation Using 21 cm Radiation from the Epoch of Reionization*, *Astrophys. J.* **653** (2006) 815 [[astro-ph/0512263](#)].
- [89] S. R. Furlanetto and A. Lidz, *The Cross-Correlation of High-Redshift 21 cm and Galaxy Surveys*, *Astrophys. J.* **660** (2007) 1030 [[astro-ph/0611274](#)].
- [90] A. Lidz, O. Zahn, M. McQuinn, M. Zaldarriaga and L. Hernquist, *Detecting the Rise and Fall of 21 cm Fluctuations with the Murchison Widefield Array*, *Astrophys. J.* **680** (2008) 962 [[0711.4373](#)].
- [91] J. S. B. Wyithe and M. F. Morales, *Biased reionization and non-Gaussianity in redshifted 21-cm intensity maps of the reionization epoch*, *Mon. Notices Royal Astron. Soc.* **379** (2007) 1647 [[astro-ph/0703070](#)].
- [92] J. Pritchard, K. Ichiki, A. Mesinger, R. B. Metcalf, A. Pourtsidou, M. Santos et al., *Cosmology from EoR/Cosmic Dawn with the SKA*, in *Advancing Astrophysics with the Square Kilometre Array (AASKA14)*, p. 12, Apr., 2015, [1501.04291](#).
- [93] T. C. Chang, Y. Gong, M. Santos, M. B. Silva, J. Aguirre, O. Doré et al., *Synergy of CO/[CII]/Lya Line Intensity Mapping with the SKA*, in *Advancing Astrophysics with the Square Kilometre Array (AASKA14)*, p. 4, Apr, 2015, [1501.04654](#).
- [94] Planck Collaboration, P. A. R. Ade, N. Aghanim, M. Arnaud, F. Arroja, M. Ashdown et al., *Planck 2015 results. XX. Constraints on inflation*, *Astron. Astrophys.* **594** (2016) A20 [[1502.02114](#)].